Biosensors and Bioelectronics 72 (2015) 370–375

Contents lists available at ScienceDirect

Biosensors and Bioelectronics

journal homepage: www.elsevier.com/locate/bios

U-shaped fiber-optic ATR sensor enhanced by silver nanoparticles for continuous glucose monitoring

Dachao Li [a,*], Songlin Yu [b], Changyue Sun [c], Chongwei Zou [a], Haixia Yu [c], Kexin Xu [a]

[a] State Key Laboratory of Precision Measuring Technology and Instruments, Tianjin University, 92 Weijin Rd., Nankai District, Tianjin 300072, PR China
[b] Temperature Laboratory, Tianjin Institute of Metrological Supervision Testing, 4 Keyanxi Rd., Nankai District, Tianjin 300192, PR China
[c] Tianjin Key Laboratory of Biomedical Detecting Techniques and Instruments, Tianjin University, 92 Weijin Rd., Nankai District, Tianjin 300072, PR China

ARTICLE INFO

Article history:
Received 16 February 2015
Received in revised form
9 May 2015
Accepted 9 May 2015
Available online 11 May 2015

Keywords:
Continuous glucose monitoring
Fiber-optic ATR sensor
U-shaped structure
Silver nanoparticle
Cylindrical surface

ABSTRACT

An implantable U-shaped fiber ATR sensor enhanced by silver nanoparticles on cylindrical surface was presented for continuous glucose monitoring to overcome the drawbacks of traditional glucose sensing technique based on enzyme electrodes. A U-shaped structure was addressed to increase effective optical length at limited implantable space to enhance the sensitivity of fiber ATR sensor. A novel method to fabricate silver nanoparticles on cylindrical surface of U-shaped fiber ATR sensor based on chemical reduction of its silver halide material directly without any preliminary nanoparticles synthesis and following covalent bond or self-assembly was proposed. Five glucose absorption wavelengths in the mid-infrared band were employed for specific glucose monitoring. The experimental results indicate that the sensitivity and resolution of the silver-nanoparticle-enhanced U-shaped fiber-optic ATR sensor are approximately three times those of a conventional one. The high sensitivity and low-noise performance makes it promising for in vivo glucose monitoring in the future clinical applications.

1. Introduction

Diabetes mellitus is a serious human disease, and it is important to monitor blood glucose levels continuously to provide guidance for diagnosis and therapy. To date, the implantable enzyme electrode sensing technique is the only method that has been used in clinical settings for continuous glucose monitoring by measuring the electric current generated by enzyme reactions in subcutaneous tissue (Oliver et al., 2009). The representative products include SEVEN® Plus (DexCom, Inc.) (Zisser et al., 2009), Paradigm® REAL-Time (Medtronic, Inc.) (Deiss et al., 2006) and FreeStyle Navigator® (Abbott Laboratories) (Weinzimer et al., 2008). However, the significant drift caused by bioelectricity and the effect of electrochemical reactions under hypoxia reduce the accuracy of glucose monitoring. Therefore, finger-prick blood corrections are often required to calibrate enzyme-based glucose sensors several times each day. In addition, the local glucose level close to the enzyme electrode is irreversibly depleted by the glucose oxidase enzyme reaction, resulting in a measured glucose value that is lower than the true concentration. Especially, it is difficult to detect the hypoglycemia effectively using enzyme electrode based sensors, which is still a big challenge for continuous glucose monitoring in clinics. The fluorescence-based glucose sensors have ever showed its potential for glucose in vivo (He et al., 2014). However, this method is vulnerable for slow response time and poor long-term stability of fluorescent molecules. Also biomolecules similar to glucose may cause interferes and give false positives. The surface-enhanced Raman scattering (SERS), a very promising technique for glucose sensing, has been investigated for glucose determination in physiological concentration range (Chanda et al., 2004; Kong et al., 2014). However, the biggest challenge of this technique of how to miniaturize the SERS-active surface and fabricate active substrate on the tip of a fiber-optic probe for implantable glucose determination.

The glucose “finger print” band has been successfully applied for direct glucose monitoring in vitro from bio-fluid with complex components such as blood, interstitial fluid (ISF) and dialysis solution by mid-infrared ATR spectroscopy (Diessel et al., 2005; Lambrecht et al., 2006; Roychoudhury et al., 2006). At the same time, the fiber-based technique provides an excellent approach to fabricate small ATR sensors, which makes it possible to implant the sensors into subcutaneous tissue for continuous glucose monitoring (Yu et al., 2014). Compared with enzyme electrode sensors, only light was allowed to pass though the implantable fiber-optic sensor under the skin, therefore the glucose monitoring using fiber-optic sensors is not affected by bioelectricity in the body. The glucose “finger print” absorption peaks were used for specific glucose monitoring instead of oxidase enzyme, so the

* Corresponding author. Tel.: +86 22 27403916; fax: +86 22 27406726.
E-mail address: dchli@tju.edu.cn (D. Li).

http://dx.doi.org/10.1016/j.bios.2015.05.023
0956-5663/

affection of glucose depleted by enzyme reaction was avoided, then it is possible to detect the hypoglycemia which will bring deadly dangerous for diabetics, and the glucose concentration measured is more consistent with the actual value. Compared with the fluorescence-based glucose sensor, the sensor fabricated in this paper need not be banded to any fluorescent molecules and the specific absorbance in the mid-infrared band allows a substance to be distinguished from various chemical species. These characteristics make the fiber-optic ATR sensor more suitable and promising for implantation in tissue for continuous glucose monitoring. However, low sensitivity and resolution are concomitant with the miniaturization of the fiber-optic ATR sensor.

To improve the sensitivity and monitoring resolution of fiber-optic ATR sensor, a U-shaped fiber-optic ATR sensor was fabricated in this study. The bent structure was constructive to increase the sensing optical length of the fiber-optic sensor in a limited space for implantable glucose measurement (Raichlin and Katzir, 2008). Compared with those of the conventional straight fiber-optic ATR sensor, each penetration depth and the total number of reflections were both increased after the fiber was bent (Artyushenko et al., 2008). Thus, the sensitivity and measurement resolution were improved.

Further, the silver nanoparticles were used to modify the surface of the U-shaped fiber-optic ATR sensor to enhance the infrared absorption of glucose. The absorption spectrum of the molecules near the nanoparticles was enhanced by a phenomenon exploited in ATR surface-enhanced infrared absorption (SEIRA) spectroscopy (Huo et al., 2009; Schnell et al., 2009). Unlike SERS, SEIRA spectrum was insensitive to the size and shape of nanoparticles. Aroca has investigated the enhanced factors of different metal nanoparticles and their SEIRA spectrums show no wavelength shift (Aroca, 2006). Thus, how to prepare SEIRA-active nanoparticles on the surface of sensor and improve the enhanced factor is the most concerned focus in SEIRA study. To date, studies of ATR-SEIRA only concentrated on a plane substrate (Enders et al., 2011; Neubrech et al., 2008; Yan et al., 2008). Metal nanoparticles on crystalline ATR cells have been prepared through physical vapor deposition (PVD) or other deposition method (Renoirt et al., 2014; Sanchez-Cortes et al., 2001), electrode deposition methods (Magagnin et al., 2002) or wet chemical methods (Rao and Yang, 2011). However, it is a great challenge to grow metal nanoparticles with required size and distribution on the cylindrical surface of silver halide fibers and even more so to grow them on the bent fibers. In this study, the silver nanoparticles were fabricated on cylindrical surface of U-shaped fiber ATR sensor based on its silver halide material reduction directly without any preliminary nanoparticles synthesis and the following covalent bond or self-assembly for the first time. In the process of chemical reduction, glucose was employed as the reducing agent, the material of fiber ATR sensor is made of AgCl and AgBr which could offer silver ions by itself. This method provides a new way to fabricate nanoparticles on cylindrical surface of the fiber sensor based on silver halide materials.

2. Design of fiber-optic ATR sensor

2.1. Structure of implantable fiber-optic ATR sensor

As shown in Fig. 1, the silver-nanoparticle-enhanced fiber-optic ATR sensor can be implanted into subcutaneous tissue for continuous glucose monitoring. A biocompatible semipermeable membrane with a selectable molecular weight cut-off was used as a protective cover to separate the implanted sensor from the tissue, filter out large biological molecules within the ISF and allow glucose molecules to pass through. The sensor was fabricated in two main steps: (1) the design of the bent, high-sensitivity fiber-optic ATR sensor with U-shaped structure. (2) The preparation of silver nanoparticles on cylindrical surface of U-shaped fiber-optic ATR sensor. Only the sensor was inserted into tissue and the laser light pass through it for glucose sensing without interacting with the tissue.

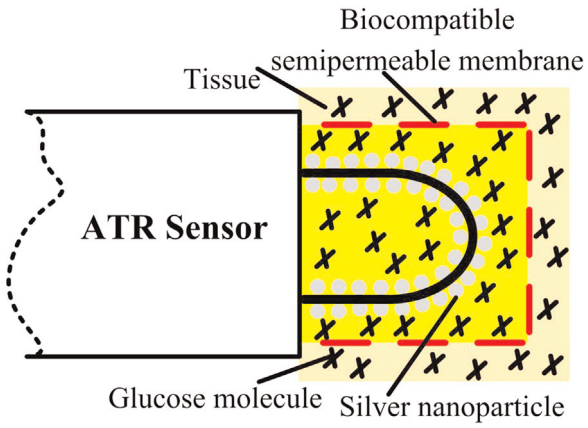

Fig. 1. Schematic diagram of implantable, silver-nanoparticle-enhanced fiber-optic ATR sensor.

2.2. U-shaped fiber-optic ATR sensor

According to the Lambert–Beer law, increasing the sensing optical length of a fiber-optic ATR sensor is conducive to improve its sensitivity because the sensing optical length is proportional to each penetration depth d_p and the total number of internal reflections N_m For a conventional straight fiber-optic ATR sensor, the penetration depth d_p and total number of reflections N_m can be determined as follows:

$$d_p = \frac{\lambda_0}{2\pi n_1[\sin^2\theta - (n_2/n_{core})^2]^{1/2}} \quad (1)$$

$$N_m = \frac{L}{2\rho}\cot\theta \quad (2)$$

where ρ is the core radius; L is the sensing length (unclad region length), θ is the angle of incidence, and n_2 is the refractive index of the measured sample. Because $n_2 \ll n_{core}$ and L, P and the numerical aperture of the fibers are restricted, the sensitivity and resolution of straight fiber-optic ATR sensors are low. A bent sensor could be used to increase the number of reflections and the penetration depth at each reflection, leading to the increase of the effective sensing optical length, i.e., the sensitivity was increased.

According to the previous study (Artyushenko et al., 2008), the sensitivity of bent fiber-optic ATR sensor could be expressed by the ratio of effective evanescent absorption coefficient and bulk absorption coefficient of fluid surrounding the sensor. The numerous excellent properties of polycrystalline infrared (PIR) fibers (A.R.T. Photonics GmbH, Berlin, Germany), such as a broad transmission band (4–18 μm), non-hygroscopic behavior, and the lack of brittleness and toxicity, have enabled their widespread use in biosample measurement. The refractive indices of the core and cladding were 2.15 and 2.13, respectively. The sensitivity of bent fiber-optic ATR sensor was proportional to the fiber-core radius and inversely proportional to bent radius. As the bent fiber-optic ATR sensor will be implanted in the tissue, its measurement sensitivity and size should be weighted and optimized. Finally, the multimode silver halide PIR fibers with an outer diameter of 700 μm and a core diameter of 630 μm were chosen as the materials, and a U-shaped fiber-optic sensor with a bent radius of 2.5 mm was fabricated in this paper.

2.3. Enhancement of fiber ATR sensor by silver nanoparticles

Metal nanoparticles have been successfully used to enhance the molecular absorption spectrum in mid-infrared named as SEIRA (Ataka and Heberle, 2007; Pronkin and Wandlowski, 2003). According to electromagnetic enhancement theory of SEIRA, the enhancement factor depended on the size, shape and distribution of metal particles on the substrate (Aroca, 2006). The tabular shaped metal islands, especially in a dense nanoparticle array locally confined areas, huge electromagnetic enhancement occurred (Enders et al., 2011; Wang et al., 2013). In this paper, silver nanoparticles were used to modify the fiber-optic surface to enhance glucose absorption spectrum. However, it is very difficult for the traditional method, such as PVD and electrode deposition, to prepare metal nanoparticles on the cylindrical surface of bent fiber-optic ATR sensor. In this paper, a chemical reduction method was creatively introduced to prepare silver nanoparticles on the PIR fiber (composed of $AgCL_xBr_{1-x}$) (Artjushenko et al., 2005) cylindrical surface from the fiber material composition for the first time.

2.4. Specific determination of glucose using tunable laser

A tunable laser was employed as the light source to improve the measurement resolution of the designed sensor because of the laser's high peak power and high spectral resolution (Brandstetter and Lendl, 2012; Brandstetter et al., 2013). However, the absorption spectrum of urea, urea acid, creatinine, phosphate and other materials in blood or interstitial fluid overlapped with the glucose absorption spectrum (Jax et al., 2011; Martin et al., 2005), which is the biggest challenge for glucose monitoring using spectral method, especially for single or two wavelengths spectrometer. Therefore, at least 3–5 working wavelengths were needed to overcome the spectral interference presented by other substances and achieve high-precision glucose monitoring from ISF using spectral analysis (Pleitez et al., 2012; Vrančić et al., 2011). In this paper, five emission wavelengths, 1081, 1076, 1051, 1041 and 1037 cm^{-1}, in the glucose "finger print" band were tuned and stabilized as the working wavelengths for glucose monitoring. These multiple working lines will be powerful and sufficient to identify glucose from other materials in interstitial fluid and achieve specific monitoring of glucose and these multiple work wavelengths are able to reduce the interference of other components and improve the measurement accuracy. The interference by the other components in body fluid for glucose identification has been fully investigated in the pervious studies (Pleitez et al., 2012; Vrančić et al., 2011). What is more, no enzyme is needed. Therefore, both interference from bioelectricity and the irreversible depletion of glucose are avoided.

3. Preparation and evaluation of silver nanoparticles

3.1. Method of silver nanoparticles preparation

Glucose was employed as the reducing agent, and the chemical reduction reaction between ions in the fiber material can be expressed as follows (Rao and Yang, 2011):

$$Ag^+Cl^- + Ag^+Br^- + CH_2OH(CHOH)_4CHO + NaOH \rightarrow Ag + CH_2OH(CHOH)_4COOH + Na^+Cl^- + Na^+Br^- \quad (3)$$

The concentration of glucose with aldehyde groups (–CHO) is very low (Supplementary Fig. 1). However, the silver ions can be reduced by –CHO at normal temperature in alkaline solution (PH value varies around 12), which strongly influences the nanoparticles morphology and hence the SEIRA signals. In week alkaline solution, the Ag ion can not be reduced as Ag atom. That is to say, the glucose in body fluid (normal blood pH varies between 7.35 and 7.45) will not change the nanoparticles morphology of the implanted fiber-optic sensor. A sodium hydroxide (NaOH) reagent was added to the reaction solution to adjust the PH value. The added alkaline reagent caused the reduction reaction to take place at room temperature and enhanced the reduction ability of –CHO. The temperature was controlled by a water bath to stabilize the reaction conditions. The optimal conditions were observed to be the addition of 15 mM NaOH to 0.25 mM glucose solutions, and the reaction times were observed to be 100 min and 80 min respectively. Then silver nanoparticles could be fabricated on the cylindrical surface of bent fiber ATR sensor based on chemical reduction of its silver halide material directly. Thus, any preliminary nanoparticles synthesis and the following covalent bond or self-assembly would not be required.

3.2. Materials and experimental procedure

Sodium hydroxide and glucose were purchased from Jiangtian Chemical Technology Co., Ltd. (Tianjin, China) and Guangfusci. Co., (Tianjin, China), respectively. All of the chemicals were dissolved in deionized water. Only the sensing part (bent region) of the U-shaped fiber-optic ATR sensor was placed in a beaker containing specified concentrations of the reducing agent and sodium hydroxide. After the desired reaction time, the sensor was taken out and immersed in deionized water for 1–2 min to stop the reaction. The reaction time was optimized and determined as follows: (1) when the reducing agent concentration as 0.25 mM, the total reaction time was 80 min. After 30 min of reaction time, the sensor was taken out and dipped into deionized water for 1 min, then immersed in the reaction solution again. The sensor was then washed 55 min after the reaction began. (2) When the reducing agent concentration was 0.15 mM, the total reaction time was 100 min; the sensor was then washed 40, 60 and 80 min after the reaction began. The entire experimental procedure was performed in a dark room to prevent the degradation of the silver halide fiber.

3.3. Evaluation of silver nanoparticles

The size and distribution of the silver nanoparticles grown on the cylindrical surface of the fiber-optic ATR sensor were preliminarily evaluated using a scanning electron microscope (Nanosem 430, FEI Co., Oregon, USA). The experimental results are shown in Fig. 2(a) (reducing agent: 0.15 mM; NaOH: 15 mM) and 2 (b) (reducing agent: 0.25 mM; NaOH: 15 mM). As shown in Fig. 2 (a), a reducing agent concentration of 0.15 mM led to sparse and clustered silver nanoparticles, which may have been caused by the low rate of silver atom reduction due to the low concentration of –CHO. As the concentration of –CHO increased with the concentration of the reducing agent, many silver atoms were reduced, yielding nanoparticles of different sizes and shapes. The sizes of these nanoparticles were generally between 85 and 140 nm. As the reducing agent concentration increased, the nanoparticles were stacked (data not shown). According to previous studies, stacked nanoparticles exhibit low SEIRA activity.

A water bath (25 °C) was employed to further control the temperature and thereby strengthen the repeatability of the chemical reducing method. According to previous studies, nanoparticles reduced by 0.25 mM reducing agent and 15 mM NaOH appeared to be more SEIRA-active than those reduced by 0.15 mM reducing agent and 15 mM NaOH (Rao and Yang, 2011). The following section will focus on the former experimental conditions. Nanoparticles distributed on the surface of the silver halide fiber are shown in Fig. 3. Most of nanoparticles were nearly spherical in

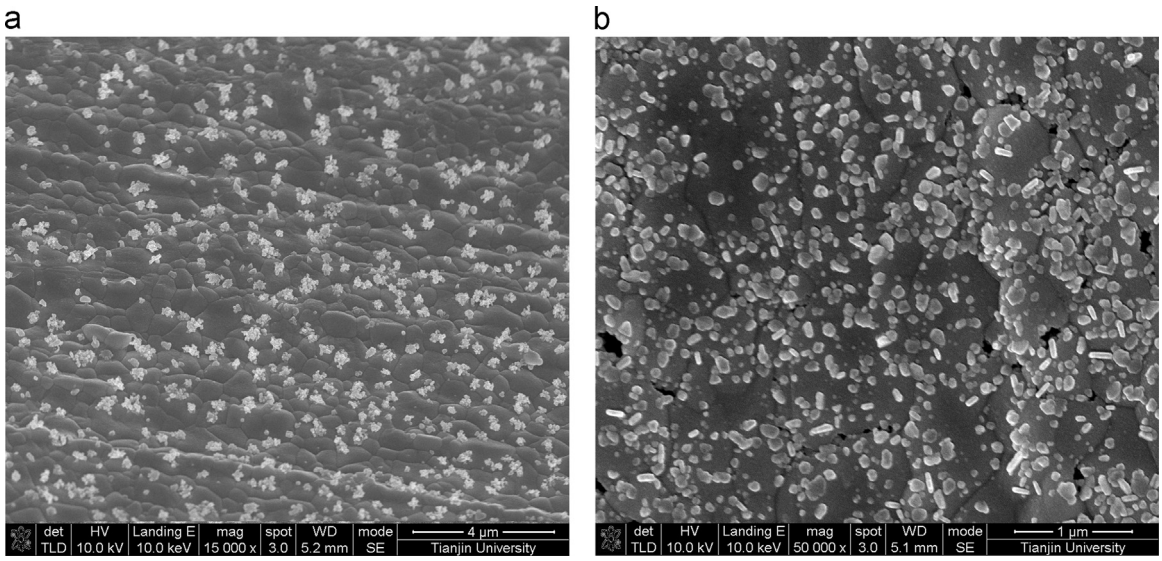

Fig. 2. SEM images of nanoparticles on cylindrical surface of silver halide fiber. (a) Reducing agent: 0.15 mM; NaOH: 15 mM. The total reaction time was 100 min. (b) Reducing agent: 0.15 mM; NaOH: 15 mM. The total reaction time was 80 min.

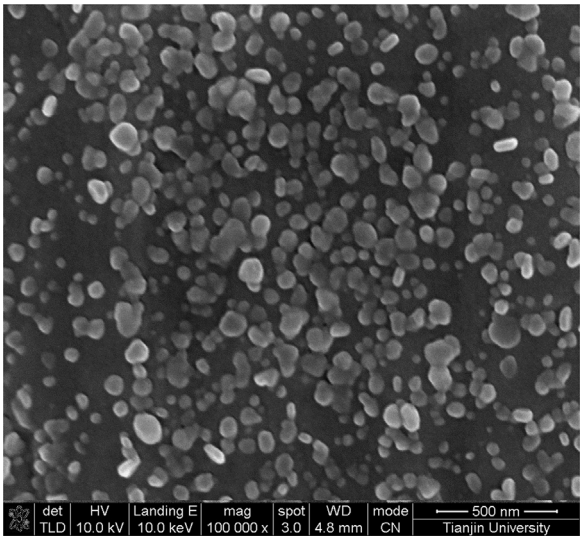

Fig. 3. Nanoparticles reduced by 0.25 mM reducing agent and 15 mM NaOH in 25 °C water bath, and the total reaction time was 80 min.

shape and measured between 60 and 100 nm, as shown in Fig. 3. A few nanoparticles were nearly ellipsoidal in shape. The long axes measured between 85 and 120 nm, and the short axes measured between 35 and 50 nm. Therefore, the axial ratio of most of the particles was between 2 and 2.5. It should be noted that most of the nanoparticles were nearly spherical, the reason for which is not clear.

4. Performance of enhanced fiber-optic sensor for glucose sensing

4.1. Experimental set-up

A dual-path laser-measurement set-up was established for glucose monitoring using a tunable CO_2 laser and fiber-optic ATR sensor (Supplementary Fig. 2). An infrared attenuator (Model 401, Lasnix, Berg, Germany) was used to attenuate the high laser output power (maximum power of 800 mW) to a reasonable level. The attenuated laser beam was divided into dual paths by a zinc selenide (ZnSe) beam splitter (BS), one for reference and the other for sample measurement. The dual-path incidence laser beams were coupled into reference and sample detectors (Det. R and Det. S) by a ZnSe lens. The two infrared detectors (LME-353, InfraTec GmbH, Dresden, Germany) were matched with two lock-in amplifiers of the same model (SR830, Stanford Research Systems, Inc., California, USA), the synchronous reference frequency (750 HZ) of which was provided by the RF circuit of the laser system. The lock-in signals of the dual paths were then recorded by a data-acquisition card synchronously.

The absorbance caused by changes in glucose concentration can be expressed as follows (Yu et al., 2013):

$$A_s = \ln(u_b^s/u_g^s) + \ln(u_g^r/u_b^r) \quad (4)$$

Where "u" is the lock-in amplified voltage, the superscripts "s" and "r" represent the sample and reference paths, respectively, and the subscripts "b" and "g" denote the background and glucose solution, respectively.

4.2. Nanoparticle-enhanced fiber-optic sensor for glucose monitoring

A conventional fiber-optic ATR sensor and a nanoparticle-enhanced fiber-optic ATR sensor were used for glucose monitoring. As shown in Fig. 4(a) and (b), the absorbance correlates well with the glucose concentration at 1081 and 1037 cm^{-1}, and the linearity of the two types of fiber-optic ATR sensors is such that $R^2 \geq 0.98$. The correlations between absorbance and glucose concentration in the low range at 1081 and 1037 cm^{-1} are presented in the insets of Fig. 4(a) and (b). The slope of the linear fit of the glucose absorbance versus the glucose concentration was employed to calculate the enhancement factor of the nanoparticles. The enhancement factors at 1081 and 1037 cm^{-1} were calculated to be $R_{1081} = 2.97$ and $R_{1037} = 3.18$, respectively. For the conventional U-shaped fiber-optic ATR sensor, the measurement resolution was approximately 45 mg/dL, whereas the measurement resolution of the silver-nanoparticle-enhanced U-shaped fiber-optic ATR sensor was approximately 15 mg/dL. People with diabetes will be unconscious if the blood glucose concentration becomes lower than 30 mg/dL in clinics. Thus the resolution of this enhanced fiber-optic ATR sensor in this paper could satisfy the clinical requirements for continuous glucose monitoring of diabetes. Jensen et al. (2003) had pointed out that the change of temperatures is

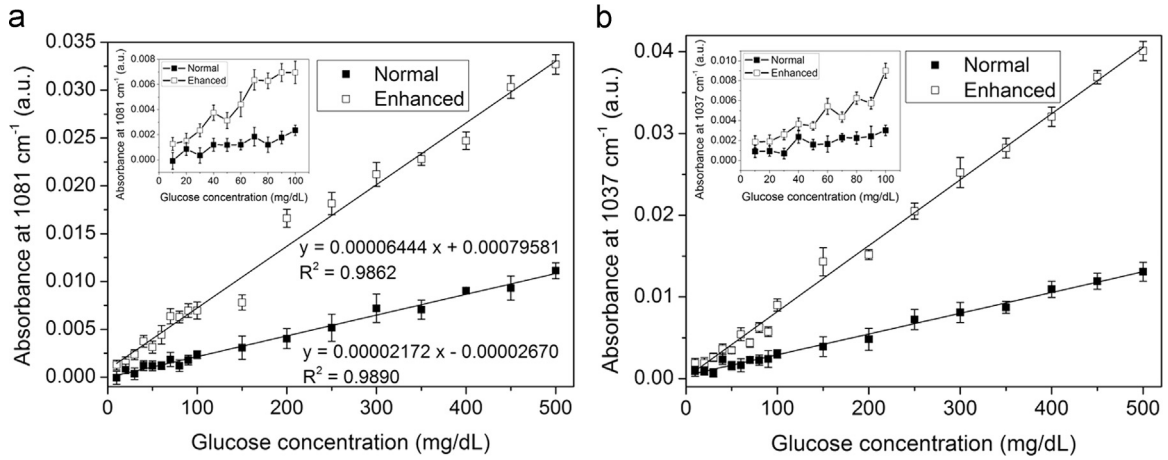

Fig. 4. Plot of absorbance vs. glucose concentration measured by conventional and silver-nanoparticle-enhanced fiber-optic sensors. (a) 1081 cm^{-1}. (b) 1037 cm^{-1}.

negligible for glucose identification using min-infrared spectroscopy, and the region between 1100 and 1000 cm^{-1} is well suited and sufficient for glucose quantitative analysis. However, many holes were formed during the growth of the silver nanoparticles on the cylindrical surface of the silver halide fiber by chemical reduction. The effects of these holes on glucose measurement should be investigated in future research.

5. Conclusions

In this study, a method for continuous glucose monitoring based on a silver-nanoparticle-enhanced bent fiber-optic ATR sensor in combination with a tunable mid-infrared laser was proposed for the first time. A U-shaped fiber-optic ATR sensor with a radius of 2.5 mm was fabricated, on which silver nanoparticles were prepared to enhance the sensitivity of the sensor using a chemical reduction method without any preliminary nanoparticles synthesis and the following covalent bond or self-assembly. In the process of chemical reduction, nanoparticles were reduced from the silver ions of fiber-optic ATR sensor itself, which provides a new way to fabricate nanoparticles on cylindrical surface of the fiber sensor based on silver halide materials. In a 25°C water bath, most of the nanoparticles were nearly spherical in shape and measured between 60 and 100 nm. A fewer nanoparticles were nearly ellipsoidal in shape with an axial ratio of 2–2.5. The long axes were measured between 85 and 120 nm and short axes between 35 and 50 nm, respectively.

Based on the conventional and silver-nanoparticle-enhanced U-shaped fiber-optic ATR sensors, a dual-path laser-measurement set-up was established. A tunable CO_2 laser, with emission wavelengths 1081, 1076, 1051, 1041 and 1037 cm^{-1} of glucose absorption was employed as the light source to achieve specific glucose monitoring and improve the measurement sensitivity. The experiment results indicate that the sensitivity and measurement resolution of the silver-nanoparticle-enhanced U-shaped fiber-optic ATR sensor are approximately three times those of the conventional one. Its high precision and high sensitivity make the system promising for continuous glucose monitoring in vivo. Future work will focus on the sensor's biocompatible encapsulation and animal experiments.

Acknowledgments

This work was supported by the National Natural Science Foundation of China (Nos. 61176107, 51350110233, 11204210, 61428402 and 61201039), the Key Projects in the Science and Technology Pillar Program of Tianjin (No. 11CKFSY01500), the Key Program of Tianjin Natural Science Foundation (No. 15JCZDJC36100), the National Key Projects in Non-profit Industry (No. GYHY200906037), the National High Technology Research and Development Program of China (No. 2012AA022602), and the 111 Project of China (No. B07014).

Appendix A. Supplementary information

Supplementary data associated with this article can be found in the online version at http://dx.doi.org/10.1016/j.bios.2015.05.023.

References

Aroca, R. 2006. Spectroscopy, Madrid.
Artjushenko, V., Baskov, P., Kuz'micheva, G., Musina, M., Sakharov, V., Sakharova, T., 2005. Inorg. Mater. 41, 178–181.
Artyushenko, V., Bocharnikov, A., Colquhoun, G., Leach, C., Lobachev, V., Sakharova, T., Savitsky, D., 2008. Vib. Spectrosc. 48, 168–171.
Ataka, K., Heberle, J., 2007. Anal. Bioanal. Chem. 388, 47–54.
Brandstetter, M., Lendl, B., 2012. Sens. Actuators B: Chem. 170, 189–195.
Brandstetter, M., Volgger, L., Genner, A., Jungbauer, C., Lendl, B., 2013. Appl. Phys. B 110, 233–239.
Chanda, Xiaoyu Zhang, C.L.H., Walsh Jr., Joseph T., Van Duyne, Richard P., 2004. Anal. Chem. 76, 78–85.
Deiss, D., Bolinder, J., Riveline, J.P., Battelino, T., Bosi, E., Tubiana-Rufi, N., Kerr, D., Phillip, M., 2006. Diabetes Care 29, 2730–2732.
Diessel, E., Kamphaus, P., Grothe, K., Kurte, R., Damm, U., Heise, H.M., 2005. Appl. Spectrosc. 59, 442–451.
Enders, D., Nagao, T., Pucci, A., Nakayama, T., Aono, M., 2011. Phys. Chem. Chem. Phys. 13, 4935–4941.
He, Y., Wang, X., Sun, J., Jiao, S., Chen, H., Gao, F., Wang, L., 2014. Anal. Chim. Acta 810, 71–78.
Huo, S.J., Wang, J.Y., Sun, D.-L., Cai, W.B., 2009. Appl. Spectrosc. 63, 1162–1167.
Jax, T., Heise, T., Nosek, L., Gable, J., Lim, G., Calentine, C., 2011. J. Diabetes Sci. Technol. 5, 345–352.
Jensen, P.S., Bak, J., Andersson-Engels, S., 2003. Appl. Spectrosc. 57, 28–36.
Kong, K., Ho, C.H., Gong, T., 2014. Biosens. Bioelectron. 56, 186–191.
Lambrecht, A., Beyer, T., Hebestreit, K., Mischler, R., Petrich, W., 2006. Appl. Spectrosc. 60, 729–736.
Magagnin, L., Maboudian, R., Carraro, C., 2002. J. Phys. Chem. B 106, 401–407.
Martin, W.B., Mirov, S., Venugopalan, R., 2005. Appl. Spectrosc. 59, 881–884.
Neubrech, F., Pucci, A., Cornelius, T.W., Karim, S., García-Etxarri, A., Aizpurua, J., 2008. Phys. Rev. Lett., 157403.
Oliver, N., Toumazou, C., Cass, A., Johnston, D., 2009. Diabet. Med. 26, 197–210.
Pleitez, M., von Lilienfeld-Toal, H., Mäntele, W., 2012. Spectrochim. Acta A 85, 61–65.
Pronkin, S., Wandlowski, T., 2003. J. Electroanal. Chem. 550-551, 131–147.
Raichlin, Y., Katzir, A., 2008. Appl. Spectrosc. 62, 55A.
Rao, G.P.C., Yang, J., 2011. Anal. Bioanal. Chem. 401, 2935–2943.
Renoirt, J.M., Debliquy, M., Albert, J., Ianoul, A., Caucheteur, C., 2014. J. Phys. Chem. C 118, 11035–11042.
Roychoudhury, P., Harvey, L.M., McNeil, B., 2006. Anal. Chim. Acta 561, 218–224.
Sanchez-Cortes, S., Domingo, C., Garcia-Ramos, J., Aznarez, J., 2001. Langmuir 17,

1157–1162.
Schnell, M., Garcia-Etxarri, A., Huber, A., Crozier, K., Aizpurua, J., Hillenbrand, R., 2009. Nat. Photonics 3, 287–291.
Vrančić, C., Fomichova, A., Gretz, N., Herrmann, C., Neudecker, S., Pucci, A., Petrich, W., 2011. Analyst 136, 1192–1198.
Wang, T., Nguyen, V.H., Buchenauer, A., Schnakenberg, U., Taubner, T., 2013. Opt. Express 21, 9005–9010.
Weinzimer, S., Xing, D., Tansey, M., Fiallo-Scharer, R., Mauras, N., Wysocki, T., Beck, R., Tamborlane, W., Ruedy, K., 2008. Diabetes Care 31, 525–527.
Yan, W., Feng, X., Chen, X., Hou, W., Zhu, J.J., 2008. Biosen. Bioelectron. 23, 925–931.
Yu, S., Li, D., Chong, H., Sun, C., Xu, K., 2014. Opt. Laser Eng. 55, 78–83.
Yu, S.L., Li, D.C., Chong, H., Sun, C.Y., Xu, K.X., 2013. Proc. SPIE 8591, 85910K–85911K.
Zisser, H.C., Bailey, T.S., Schwartz, S., Ratner, R.E., Wise, J., 2009. J. Diabetes Sci. Technol. 3, 1146–1154.